coatings

MDPI

Article

Luminescence Properties of Co-doped Eu^{3+}, Bi^{3+} Lu_2O_3/Polyvinylpyrrolidone Films

Ángel de Jesús Morales-Ramírez [1,4,*], Margarita García-Hernández [2], Dulce Yolotzin Medina-Velázquez [3], María del Rosario Ruiz-Guerrero [4], Fernando Juárez-López [4] and Joan Reyes-Miranda [3]

1 Instituto Politécnico Nacional, ESIQIE, UPALM S/N Col. Lindavista, Gustavo A. Madero Cd. de México C.P. 07738, México

2 Tecnológico Nacional de México-Instituto Tecnológico de Ciudad Madero, CIP, Prol. Bahía del Aldair, Av. de las Bahías, Parque Industrial Tecnia, Altamira Tamaulipas C.P. 89600, México; margarita.garcia@itcm.edu.mx

3 Universidad Autónoma Metropolitana, Departamento de Materiales, Ciencias Básicas e Ingeniería. Av. San Pablo No. 180, Col. Reynosa Tamaulipas, Cd. de México C.P. 02200, México; dyolotzin@correo.azc.uam.mx (D.Y.M.-V.); joremi@live.com.mx (J.R.-M)

4 Instituto Politécnico Nacional, CIITEC, UPALM S/N Col. Lindavista, Gustavo A. Madero Cd. de México C.P. 07738, México; maruizg@ipn.mx (M.d.R.R.-G.); fjuarezl@ipn.mx (F.J.-L.)

* Correspondence: amoralesra@ipn.mx; Tel.: + 52-55-5729-6000 (ext. 55127)

Received: 12 October 2018; Accepted: 21 November 2018; Published: 27 November 2018

Abstract: The effect of the polyvinylpyrrolidone (PVP, M_W = 130,000) molar content, PVP/Lu = 1, 2.5, 4 and 5; on the photoluminescent and structural properties of sol-gel derived Lu_2O_3:Eu^{3+}, Bi^{3+} has been analyzed. Thin hybrid films were deposited by means of the dip-coating technique on silica quartz substrates. Films deposited at 700 °C presented a cubic structure, with non-preferential orientation, even with the presence of PVP. The photoluminescence (PL) spectrum and Comission Internationale de l'Éclairage (CIE) chromaticity diagram of films revealed a reddish Eu^{3+} emission at 612 nm ($^5D_0 \rightarrow {}^7F_2$) with an excitation at 320 nm of the Bi ions ($6s^2 \rightarrow 6s6p$), showing a highly-effective energy transfer process form Bi^{3+} to Eu^{3+} luminescent centers. On the other hand, the color temperature of the samples is strongly dependent on the PVP content, as a consequence of the observed difference on the branching ratios of $^5D_0 \rightarrow {}^7F_J$ transitions of europium ions. Lifetime studies present two different behaviors for the thin films: A non-exponential nature for the lower PVP contents, and a simple exponential nature for the highest PVP one, showing that the PVP tends to promote a better dissolution of segregates and, therefore, increases the lifetime of the Eu^{3+} emission.

Keywords: Lu_2O_3; co-doped Eu^{3+}, Bi^{3+}; photoluminescence; polyvinylpyrrolidone (PVP)

1. Introduction

The design of new functional hybrid films had an extended development in the last years due their new properties as a result of the addition of an organic to an inorganic film that combine the properties of both materials [1–5]. For example, due to polymeric properties, the hybrid films are "softer" and more flexible in their structure of all inorganic films that produce crack-free hybrid films. In this way many complexes, like citric acid (CA) ethylenediame tetra-acetic acid (EDTA), ethylene glycol (EG), triethylenetetramine (TETA) and polyvinylpyrrolidone (PVP), were studied in order to develop new materials [6,7]. Kozuka et al. [8] discovered that the thickness of films can be increased by the addition of PVP; the PVP was thought to be hybridized through hydrogen bonding, retarding condensation and promoting structural relaxation in films [8,9]. In one hand, there have been great interests in the thin films preparation of phosphors with improved physical and emissive properties.

The cubic sesquioxides (R_2O_3, R = Lu, Gd, Ln, etc.) present high thermal conductivity, physical and chemical stability, optical properties (low phonons) and the possibility of doping with RE^{3+}, which are promising for several luminescent devices [10,11]. Among them, Lu_2O_3 attracted particular attention due to its high density (9.4 $g \cdot cm^{-3}$) and high luminescence efficiency [12,13], furthermore, when doped with Eu^{3+} it has been proposed for several practical applications, including X-ray scintillator [14,15] or photoluminescent red phosphor [16]. On the other hand, it has been stated that new luminescent materials, particularly white-LEDs devices, must be capable of absorbing light in the 370–410 nm range in order to be coupled with UV-diodes as excitation source [17,18]. For this, an alternative is to co-dope the Lu_2O_3: Eu^{3+} matrix with Bi^{3+} ions [19–21], since its $6s^2 \rightarrow 6s6p$ excitation band can be used to harvest near-ultraviolet (UV) light [22]. In this regard, Chen et al. [23] analyzed the energy transfer from Bi^{3+} to Eu^{3+} in $SrLu_2O_4$: Eu^{3+}, Bi^{3+} powders. At first, they found that the emission intensity of Eu ions increased with the bismuth incorporation, then, as europium concentration increased, the emission intensity from Bi^{3+} decreases, showing the energy transfer from Bi^{3+} to Eu^{3+} [23]. Wang et al. [24] reported that at low Eu content (0.05–0.1 at.%), in $NaLuGeO_4$:1.1% Bi^{3+}, *y*% Eu^{3+} samples, there is no energy transfer from Bi to Eu, however, after 0.5 Eu^{3+} at.% the emission intensity from Bi decreases [24]. This last feature is also particularly important for relatively new fields in luminescent materials such as label in fluoroimmune assays [25], biosensors for detecting bacteria [26] or in silicon-based solar cells for down-conversion luminescence from near-UV into Vis/NIR [27,28]. To produce these new materials, the sol-gel method has been proposed, since it presents several advantages, including high purity, ultra-homogeneity, low processing temperature and the possibility to produce transparent films [29,30] and, also, it has been applied for the synthesis of photoluminescent doped-Lu_2O_3 thin films [31,32]. On the other hand, there are several methods to produce films for luminescent devices. The sol-gel is one of the widely used methods in the synthesis of phosphor films as it allows the preparation of films with high thickness due to repetitive layer deposition and to control the morphology of the final product. However, for this method it is difficult to achieve the thickness without cracking and with high optical quality [33], an effect that can be overcome with the use of PVP. Furthermore, sol-gel systems are very effective in preparing crack-free thin films and increment thickness [34–36]. In the present work, transparent Lu_2O_3:Eu^{3+}, Bi^{3+} thin films were synthesized using containing PVP-solution via the dip-coating method on quartz substrates. The structure and photoluminescent properties were analyzed as a function of the PVP content.

2. Materials and Methods

Lu_2O_3:Eu^{3+}, Bi^{3+} with PVP hybrid thin films were synthetized using the sol-gel method and dip-coating technique. First, lutetium-nitrate ($Lu(NO_3)_3$, Alfa Aesar, Ward Hill, MA, USA, 99.9%) was dissolved in ethanol (C_2H_6O, Fermont, CDMX, México, 99.5%) under vigorous magnetic stirring at 60 °C, obtaining a sol of 0.25 M lutetium concentration. Europium nitrate $Eu(NO_3)_3 \cdot 5H_2O$ (99.5%, Alfa Aesar) was incorporated in order to obtain 2.5 mol.% Eu^{3+} samples. Bismuth was incorporated from a solution prepared with the dissolution of bismuth nitrate $Bi(NO_3)_3 \cdot 5H_2O$ (98%, Sigma-Aldrich, St. Louis, MO, USA) on a 1:1 molar ratio of ethanol:diethyleneglycol ($C_4H_{10}O_3$, 98%, Sigma-Aldrich) and Bi^{3+} 0.05 M concentration. Later, a fixed volume was incorporated into the lutetium-nitrate sol in order to obtain a Bi^{3+} 1.0 mol.% doping-level. This bismuth content was selected as a result of our previous work [37] where it analyzed the effect of the bismuth concentration on the photoluminescent properties of Lu_2O_3:Eu^{3+}, Bi^{3+} powders, showing that the highest emission intensity was at Bi^{3+} 1 mol.%. The pH = 4 was adjusted with acetic acid 0.01 M solution, ($C_2H_4O_2$, Fermont, 98%), 0.27 mol 2-4-pentanedione ($C_4H_8O_3$, Sigma-Aldrich, 99%) was added as chelating agent and 3.1 mol of diethyleneglycol as stabilizer. After 4 h, polyvinylpyrrolidone, (PVP $(C_6H_9NO)_n$, M_W = 130,000 $g \cdot mol^{-1}$), was slowly incorporated into the sol with a PVP/Lu molar ratio in the range of 1–5. It is important to notice that, using the present methodology, the sample containing a molar ratio of PVP/Lu = 5 possessed the largest amount of PVP which the system could dissolve without losing the stability of the sol. The final sol was stirred for 24 h at 50 °C to obtain the completely dissolution of the PVP. For the dip-coating procedure, the sols were filtered using a 0.2 μm filter, and carefully cleaned silica glass

substrates (QSI quartz, Quartz Scientific Inc., Lake County, OH, USA, refractive index = 1.417) were dipped into the prepared sol and pulled up at a constant rate of 4 cm·s^{-1}. After each dipping, the films were dried at 100 °C for 10 min to remove the water and the most volatile organics components. Subsequently, the film was heat treated at 300 °C and 500 °C for 10 min each in order to remove the organic remnants. The dipping cycle was repeated 3 times. Finally, in order to crystallize the cubic Lu_2O_3 phase, the films were annealed at 700 °C, 800 °C and 900 °C for 3 h.

Infrared (IR) spectra were recorded in the 4000–450 cm^{-1} range using a Fourier transform infrared spectroscopy (FT-IR 2000, Perkin Elmer, Waltham, MA, USA, 2.0 cm^{-1} resolution) and using the KBr discs method with sol-gel derived powders. The structure was determined by a D2 Phase-Bruker diffractometer (Bruker, Karlsruhe, Germany) using a copper anticathode at 40 kV and 20 mA. The morphology studies were carried out in a JSM-7800F (JEOL, Tokyo, Japan) Schottky Field Emission Scanning Electron Microscope and the surface roughness of the films was measured by a tapping mode using a Nanosurf, Naio AFM (Liestal, Switzerland). Finally, the emission spectra of the films were obtained under ultraviolet (UV) excitation from a 75-W xenon lamp. The fluorescent emissions were analyzed with an Acton Pro 3500i monochromator (Acton Research Corporation, Sarasota, FL, USA) and a R955 Hamamatsu photomultiplier tube (Hamamatsu Photonics, Hamamatsu, Japan) for visible emissions. Lifetime analysis was carried out in a fluorescence spectrophotometer Hitachi F-7000 (Hitachi, Tokyo, Japan), equipped with a 150 W xenon lamp.

3. Results

3.1. Structural Studies

In order to observe the xerogel chemical evolution during the annealing process of the Lu_2O_3:Eu^{3+}, Bi^{3+} PVP modified films, a Fourier transform infrared spectra of the powder dried at 100 °C was carried out for the molar ratio of PVP/Lu = 5 sample, using the KBr pelleting method for processed powders at different annealing temperatures for 1 h, as shown if Figure 1. At 100 °C, the strong band centered at 3400 cm^{-1} corresponds to the absorption bond of alcohol stretch O–H, of ethanol and diethyleneglycol. Also, the absorption bands at 1086 cm^{-1} and 878 cm^{-1}, are ascribed to the symmetrical stretching of C–O and the deformation vibrations of C–O in CO_3^{2-} groups, respectively, and are products of the thermal decomposition of the carbonyl groups from acetic acid and diethyleneglycol.

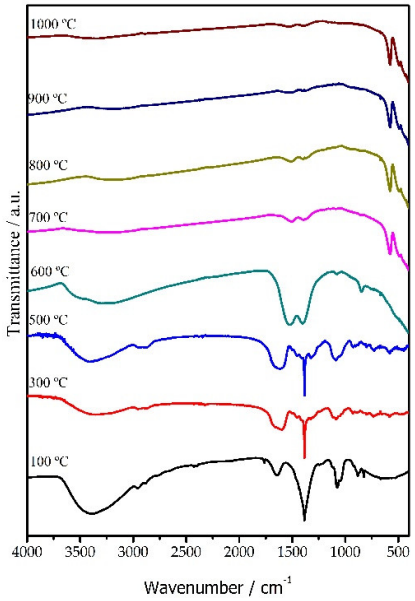

Figure 1. Fourier transform infrared spectroscopy (FT-IR) of the Lu_2O_3: Eu^{3+}, Bi^{3+} (PVP/Lu = 5.0) powder heat treatment at different temperatures.

The strong absorption band centered at 1375 cm^{-1} was ascribed to the N–O stretching vibration [38] of NO_3^- groups from the metal precursors. The band observed at 1660 cm^{-1} can be ascribed to the C=O groups of pure PVP [39]. The intensity of all these bands decreases with the increment of the annealing temperature and almost all the carbonyl groups are eliminated at 800 °C and beyond, and here only oxidized groups can be expected. Finally, the bands occurring at approximately 580, observed from 700 °C, are attributed to the Lu–O stretching vibrations of cubic Lu_2O_3 [40]. Similar results have been observed for the molar ratio of PVP/Lu = 1.0, 2.5 and 4.0 samples (not shown), and non-difference from the PVP content was detected from the previous observations.

Figure 2a,b illustrates the X-ray diffraction patterns of the Lu_2O_3:Eu^{3+}, Bi^{3+}/PVP modified thin films, for molar ratio PVP/Lu = 1 and 5, respectively, as a function of the annealing temperature. It was important to analyze these concentrations as they are the minimum and maximum molar ratio of PVP/Lu values incorporated into sol Lu_2O_3:Eu^{3+}, Bi^{3+}. As observed, the crystallization process starts when the xerogel is calcined at 600 °C, and well-defined diffraction peaks appear from 700 °C, which can be indexed to cubic Lu_2O_3 structure (JCDPS card# 431021) with a spatial group Iā3 (lattice parameter 10.391 Å), and confirms the FT-IR results showed previously. As the temperature increases, the diffraction peaks become slightly sharper and more resolved, and no new crystalline phase appears, none-from the presence of Eu^{3+} and Bi^{3+} ions, or for the PVP content.

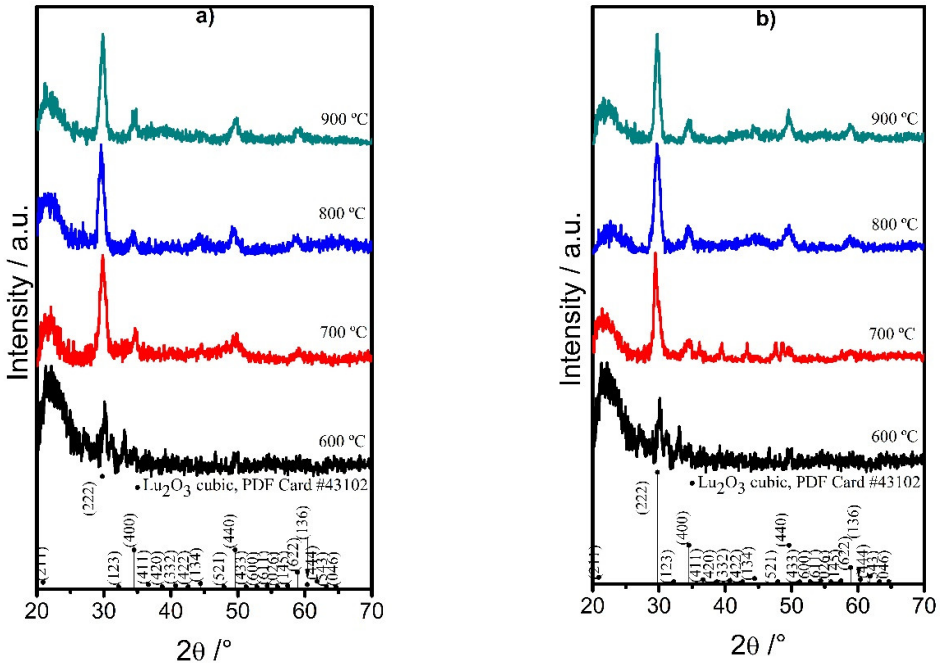

Figure 2. X-ray diffraction (XRD) patterns of Lu_2O_3:Eu^{3+}, Bi^{3+} powder at a PVP/Lu molar ratio of 1.0 (**a**) and 5.0 (**b**) heat treated at different temperatures for 1 h.

3.2. Morphology of Thin Films

The crystallite size D of the films was estimated using Scherrer's equation [34], and ranges from 8 to 11 nm, and from 7 to 11 nm, for the PVP/Lu = 1.0 and 5.0, respectively. This small crystallite size could be related to the fact that PVP tends to bind to metal ions during the sol-gel process, limiting the growing of the grains [41,42]. However, they are very similar in both samples which leads us to believe that the PVP effect is similar in both despite the different PVP content. The XRD (X-ray diffraction) results are in agreement with the FT-IR observations (Figure 1) where at 700 °C the full elimination of organic materials and the crystallization of the films were observed and completed. From the above results, the luminescent tests were performed in the films heat treated at 700 °C.

For luminescent devices, it is important to produce films without cracks in order to diminish the scattering of light. It is therefore also important to ensure the physical homogeneity of the prepared samples. Figure 3a present a Scanning Electronic Microscopy (SEM) micrograph of a selected area of the PVP/Lu = 5.0 sample annealed at 700 °C. Here it is observed that the surface is crack free and presents the typical pore-content of thin films modified with PVP. These pores are a product of the scape of the combustion gases from the pyrolysis of the organic compounds during the annealing of the film leaving, finally, just the ceramic on the substrate. Figure 3b shows a transversal image of the same film, illustrating that the thickness of the film is approximately 150 nm. It is important to notice that, in a typical sol-gel process, the thickness of the films are less than 100 nm [9], and the observed increment is a product of the use of PVP during the synthesis.

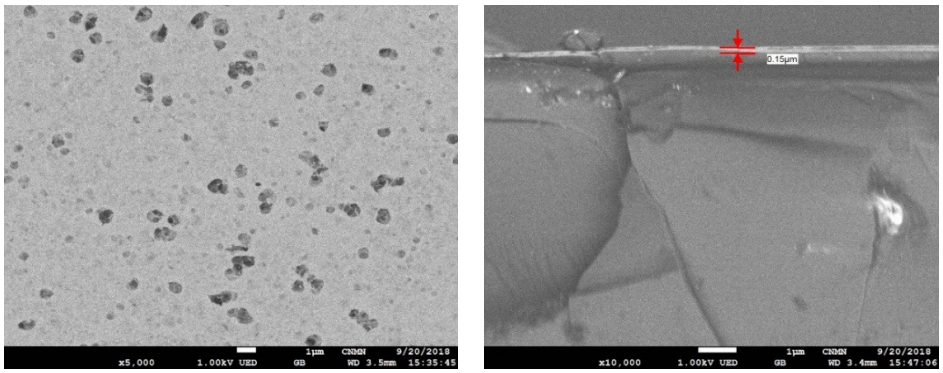

(**a**) (**b**)

Figure 3. (**a**) Scanning Electronic Microscopy (SEM) micrograph of Lu_2O_3:Eu^{3+}, Bi^{3+} thin films, PVP/Lu = 5.0, annealed at 700 °C; (**b**) SEM micrograph showing the thickness of the film. The lower cracks in the image correspond to the SiO_2 substrate.

Morphology of the films was also analyzed by AFM measurements. Figure 4 shows the micrographs for the PVP/Lu = 1.0, and 5.0 sample, annealed at 900 °C. As can be observed, in both cases the films are constituted of well-dispersed rounded grains over the entire surface. However, for the sample with the lower PVP content (PVP/Lu = 1.0), these grains are aproximately 0.5 µm, whereas in the higher (PVP/Lu = 5.0) the grain size is 1.0 µm. The difference could be explained since the PVP acts as an achelating agent during the xerogel stage and, therefore, produces the rounded morphology. It is also to be expected that the PVP promotes the agglomeration of clusters and therefore enhances their growing. However, there is no evident difference in the roughness of the films, since the RMS measurements for the PVP/Lu = 1.0 and 5.0 sample are 11.1 nm and 10.21 nm, respectively. Finally, all the samples were homogeneous and crack free.

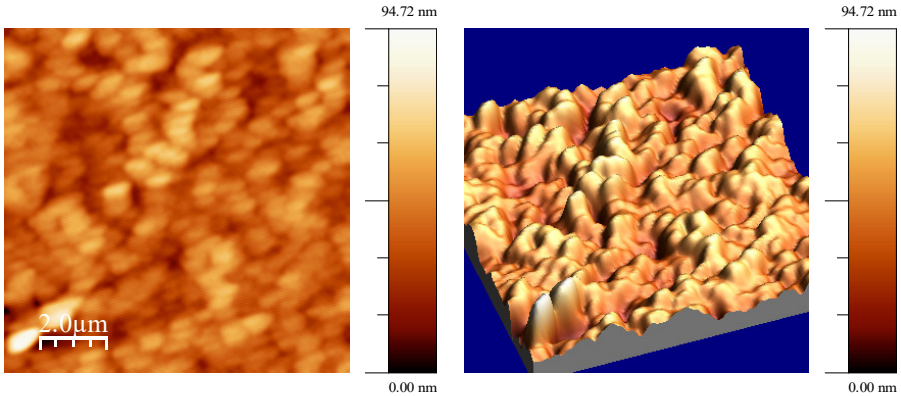

(**a**) (**b**)

Figure 4. *Cont.*

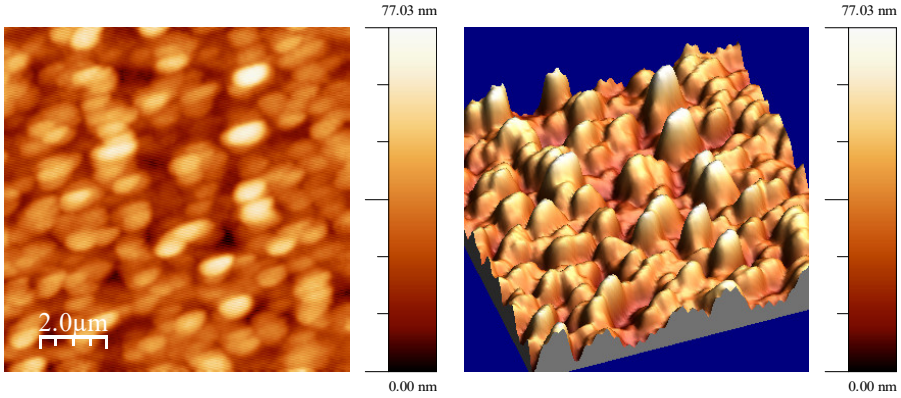

Figure 4. AFM micrographs of (**a**) PVP/Lu = 1.0, (**b**) 3D view; (**c**) PVP/Lu = 5.0 thin films, and (**d**) 3D view.

3.3. Luminescence Results and Comission Internationale de l'Éclairage (CIE) Chromaticity

Figure 5 presents the emission spectra of Lu_2O_3:Eu^{3+}, Bi^{3+} at different ratios of PVP/Lu = 1.0, 2.5, 4.0 and 5.0 heat treated at 700 °C upon excitation at 320 nm, in order to promote the energy transfer process from Bi^{3+} with $6s^2$ configuration is the $^1S_0$ [43] level, to the Eu^{3+} ions. All films presented enhanced the emission bands of Eu^{3+} which are attributed to $^5D_0 \rightarrow + \, ^7F_J$ (J = 0, 1, 2, 3 and 4) transitions of europium ions at 581, 596, 610 and 631, 657, and 688 nm, respectively. In this sense the band at 596 nm is ascribed to the Eu^{3+} magnetic dipole transition $^5D_0 \rightarrow \, ^7F_1$.

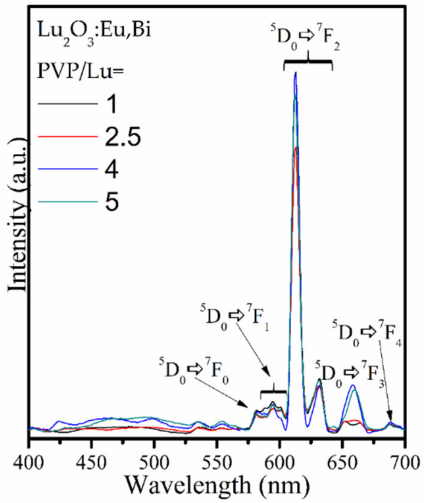

Figure 5. Emission spectra of Lu_2O_3:Eu^{3+}, Bi^{3+} films as function of PVP/Lu content. All films were annealed at 700 °C.

The band at 610 nm is attributed to Eu^{3+} electric dipole transition $^5D_0 \rightarrow \, ^7F_2$, as observed in Table 1, and the ratio R (called as the asymmetry ratio gives a measure of the degree of distortion from the inversion symmetry of the local environment of the Eu^{3+} ion in matrix) [44] between the intensities $I(^5D_0 \rightarrow \, ^7F_2)/I(^5D_0 \rightarrow \, ^7F_1)$ [45] was enhanced when the incorporation of PVP was increased. This is due to the enhancement of $^5D_0 \rightarrow ^7F_2$ which is for the magnetic dipole transition $^5D_0 \rightarrow ^7F_1$ is not sensitive to the changes in the neighborhood of the Eu^{3+} ion while the electric dipole transition $^5D_0 \rightarrow \, ^7F_2$ is very sensitive to any structural change [46]. When the molar ratio of PVP/Lu increases, the intensity of $^5D_0 \rightarrow \, ^7F_2$ transition also increases and reaches the maximum when the PVP/Lu = 4.0. Subsequently, the red luminescent intensity decreases inversely due to PVP concentration quenching, confirming that the incorporation of PVP changes the structure as shown in Figure 6 and Table 2, where the red color

purity was increased. Additionally, the transition $^5D_0 \rightarrow {}^7F_3$ at 657 nm, which is a forbidden transition, was observed for highly molar ratio of PVP. This means that the crystal field is very sensitive to the surrounding ligands and, as a result, the parity selection rules were broken [47].

It is worth noting that in the region between 400 and 600 nm, with a maximum at 550 nm a short bluish emission of Bi^{3+} ions, from the $^3P_1 \rightarrow {}^1S_0$ transition is weakly observed. This band overlaps with the typical excitation bands $^7F_0 \rightarrow {}^5L_6$ (395 nm) and $^7F_0 \rightarrow {}^5D_2$ (466 nm) of Eu^{3+} f-f interactions and, therefore, the dismissed emission of Bi^{3+} is corresponding with an effective enhancement of the Eu^{3+} emission and can be observed for all the PVP/Lu ratio due to an energy transfer process from Bi^{3+} to Eu^{3+}, as mentioned previously [48,49], in Figure 7.

Table 1. Ratio *R* or asymmetry ratio for different PVP/Lu ratios.

System	PVP/Lu	*R*
A	1.0	10.04
B	2.5	13.94
C	4.0	14.58
D	5.0	12.80

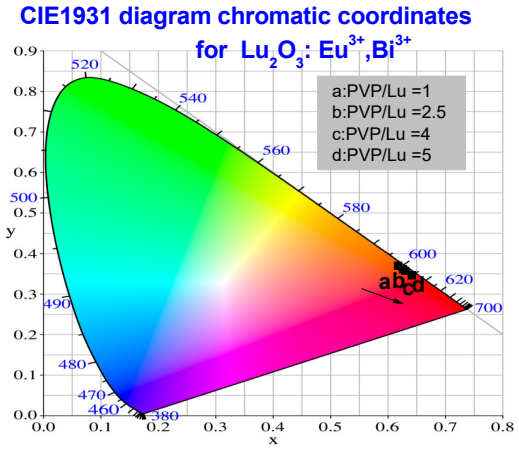

Figure 6. Comission Internationale de l'Éclairage (CIE) chromaticity coordinates for different PVP/Lu ratio. As the PVP/Lu is increased, the film CIE moves to reddish.

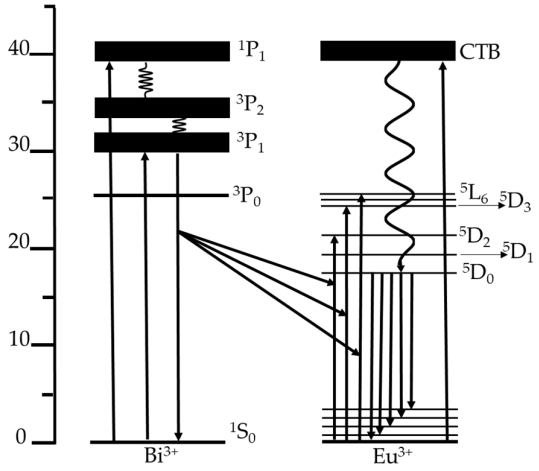

Figure 7. Energy transfer process from Bi^{3+} ion to Eu^{3+} ion.

Table 2. CIE coordinates chromaticity, color temperature and color purity for different PVP/Lu ratios.

System	PVP/Lu	*x*	*y*	Color Temperature	CP
a	1.0	0.63	0.362	1895 K	0.95
b	2.5	0.626	0.365	1829 K	0.96
c	4.0	0.618	0.374	1717 K	0.96
d	5.0	0.642	0.35	2185 K	0.97

Figure 8 shows the effect of the annealing temperature on the typical emission of the Eu^{3+} ions with a fixed content of PVP = 4.0. As can be observed, the maximum intensity is achieved at 700 °C. Since at this temperature the sample has completed the crystallization process, it is clear that at this temperature the emission process would be enhanced. It would be expected that the higher annealing temperature would promote the enhancement of the crystallinity and, therefore, the light yield of the samples. However, as can be observed at XRD results, there is not an important change in the crystallinity of the films with the increment of temperature, and only a slight increment on the crystallite size has been noted. Therefore, the diminishing of the light yield at higher annealing temperatures could be related to the growing of the structure from higher amount of impurities that change crystal structure [50,51]. Furthermore, it is known that in sol-gel films, as the temperature increases, the films begin to strongly densify and the closeness of optically active Eu ions can cause the Eu–Eu charge energy transfer. Also, this mechanism, when combined between other Eu–Eu pairs, leads to a decrease in the intensity of PL.

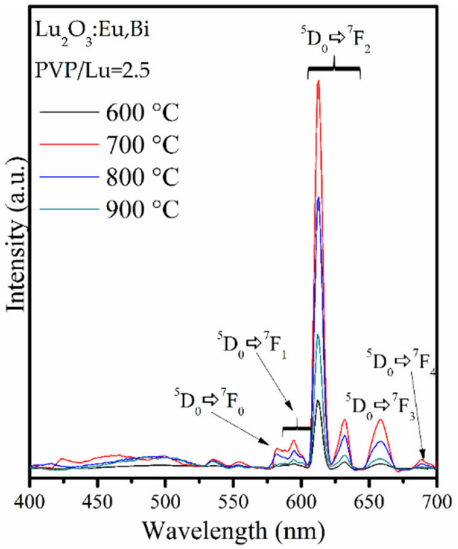

Figure 8. Emission spectra of Lu_2O_3:Eu^{3+}, Bi^{3+} films as a function of annealing temperature, PVP/Lu = 4.0.

Also Figure 6 illustrates the CIE chromaticity coordinates for different PVP/Lu ratio (1, 2.5, 4, 5). As observed, CIE chromaticity coordinates move to the reddish area by increasing the PVP/Lu ratio. The values of the computed CIE coordinates, CP (color purity) and temperature color (*K*) are listed in Table 2.

The increased PVP/Lu ratio is consistent with its higher red CP. The CP of a particular dominant color in a source is the weighted average of the (x_s, y_s) sample emission color and (x_d, y_d) dominant wavelength coordinates relative to the (x_i, y_i) illuminant coordinates. Thus, the CP compared to the CIE1931 standard [52] source C illuminant with (x_i = 0.3101, y_i = 0.3162) coordinates is given by the expression (Equation (1)) [53,54]:

$$P = \sqrt{\frac{(x_s - x_i)^2 + (y_s - y_i)^2}{(x_d - x_i)^2 + (y_d - y_i)^2}} \times 100\% \quad (1)$$

Thus, the red CP obtained from Equation (1) increases from 95% (PVP/Lu = 1) to 97% (PVP/Lu = 5), whereas the color temperature changes from 1895 to 2185 K which means that light emissions correspond to a candle flame. The branching ratio intensity (%) of the $^5D_0 \rightarrow {}^7F_J$ transitions (J = 0, 1, 2, 4) are listed in Table 3. As shown, the 1 and 2.5 PVP/Lu ratio show similar percentages in all transitions, however, when the PVP/Lu ratio is increased to 4 and 5, the $^5D_0 \rightarrow {}^7F_3$ transition exhibits a higher intensity emission, causing a reduction in the $^5D_0 \rightarrow {}^7F_2$ branching to 73%–75%. This is why the color temperature is moved to 1717 and 2185 K.

Table 3. Branching ratio intensity of the $^5D_0 \rightarrow {}^7F_J$ transitions (J = 0, 1, 2, 4) at different PVP/Lu ratios.

PVP/Lu Ratio	$^5D_0 \rightarrow {}^7F_0$	$^5D_0 \rightarrow {}^7F_1$	$^5D_0 \rightarrow {}^7F_2$	$^5D_0 \rightarrow {}^7F_3$	$^5D_0 \rightarrow {}^7F_4$
1.0	2.29	11.23	80.36	4.63	1.48
2.5	2.30	10.45	80.81	4.89	1.55
4.0	2.13	7.40	73.26	15.02	2.19
5.0	2.22	9.30	75.35	11.72	1.41

3.4. Lifetime Study

Figure 9 shows decay curves for $^5D_0 \rightarrow {}^7F_2$ (612 nm) transition under the excitation at 320 nm for samples with different PVP/Lu ratio, and Table 4 shows the resulting decay time (τ) for the analyzed samples. As can be observed, τ values are very similar for all films. However, it has been observed that for the samples with the lower PVP content (PVP/Lu = 1.0, 2.5 and 4.0), the nature of the lifetime decay curve are are non-exponential, whereas for the sample with higher PVP content (PVP/Lu = 5.0), the nature is single-exponential. This result could be related to the dissolution of segregates at high concentration of PVP [55] and therefore promotig that the films presents the higuer vale of τ. For the lower PVP content, the average lifetimes of the films which are non-exponential, were well fitted through the Inokuti Hirayama model for the multipolar interaction parameter S = 6 [56].

$$I(t) = I_0 \exp\left[-\frac{t}{\tau_0} - \gamma S\left(\frac{t}{\tau_0}\right)^{3/s}\right] \quad (2)$$

The so-called multipolar interaction parameter (S) could adopt values of 6, 8 and 10; each of them meaning dipole-dipole, dipole-quadripole, and quadripole-quadripole interactions, respectively. Form the observed results, an electric dipole-dipole interaction might be the dominant mechanism in the cross-relaxation energy transfer occurring between Eu^{3+} ions, since the direct energy transfer donor to acceptor parameter γ6 were found to be 0.31, 0.36, and 0.32 for 1, 2.5 and 4 PVP/Lu ratio, respectively.

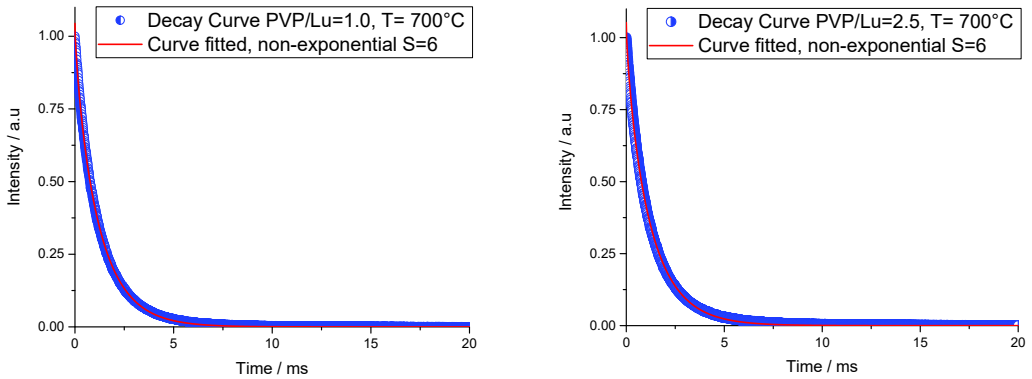

(**a**) (**b**)

Figure 9. *Cont.*

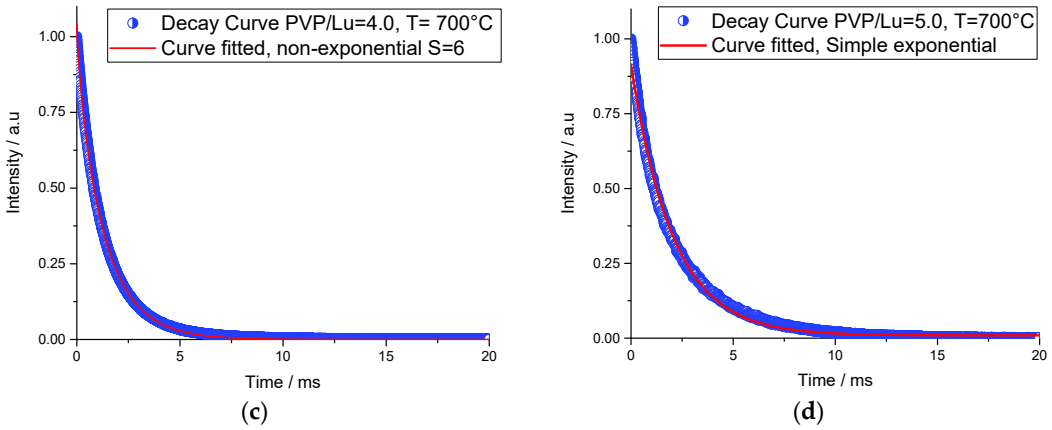

Figure 9. Decay Curves and fiting for $^5D_0 \rightarrow {}^7F_2$ (612 nm) for PVP/Lu = *X* ratio films: (**a**) *X* = 1.0; (**b**) *X* = 2.5; (**c**) *X* = 4.0; and (**d**) *X* = 5.0.

Table 4. Lifetime and non-exponential parameter for films at different PVP/Lu ratio.

PVP/Lu Ratio	τ (ms)	Parameters of Non-exponential Decay		
		R^2	*S*	γ
1.0	1.52	0.99931	6	0.32
2.5	1.58	0.99927	6	0.36
4.0	1.64	0.99934	6	0.32
5.0	2.05	0.99555	Simple Exponential	–

4. Conclusions

Lu_2O_3:Eu^{3+}, Bi^{3+} and PVP hybrid films were successfully synthesized using a different molar ratio of PVP/Lu by the sol-gel method and dip-coating technique. The films exhibited full cubic phase formation at 700 °C. Luminescence studies revealed that the films containing PVP/Lu = 2.5 presented a considerably high luminescent emission intensity of the $^5D_0 \rightarrow {}^7F_2$ transition of Eu^{3+} in the local Eu^{3+} surrounding located in the host matrix, which it is suggested for the modification generated by PVP in the elaboration of the sol into the preparation of Lu_2O_3:Eu^{3+}, Bi^{3+} films. Lifetime results show that, effectively, the PVP tends to promote a higher dissolution of Eu^{3+} ions in the host, enhancing the lifetime of the Eu^{3+} emission. The highest purity color obtained was 0.97, which made those films suitable candidates for high intensity red color applications.

Author Contributions: Conceptualization, A.d.J.M.-R; Methodology, A.d.J.M.-R., with inputs from D.Y.M.-V. and J.R.-M.; Validation, M.d.R.R.-G.; Formal Analysis, A.d.J.M.-R. with feedback from M.G.-H. and F.J.-L.; Investigation, A.d.J.M.-R. and M.G.-H.; Resources, D.Y.M.-V.; Data Curation, M.G.-H.; Writing–Original Draft Preparation, A.d.J.M.-R. and D.Y.M.-V.; Writing–Review & Editing, M.G.-H., M.d.R.R.-G. and J.R.-M.

Funding: This research was funded by CONACyT (No. 254280).

Acknowledgments: The authors thanks to Eng. Oscar Francisco Rivera Domínguez and Eng. Maribel Pacheco. We would also like to thank the Sistema Nacional de Investigadores (SNI) and to Instituto Politécnico Nacional (IPN).

Conflicts of Interest: The authors declare no conflict of interest.

References

1. Somalu, M.R.; Samat, A.A.; Muchtar, A.; Osman, N. Polymer-based approach in ceramic materials processing for energy device applications. *Acad. J. Polym. Sci.* **2018**, *1*, 555571.
2. Mir, S.H.; Nagahara, L.A.; Thundat, T.; Mokarian-Tabari, P.; Furukawa, H.; Khosla, A. Organic-inorganic hybrid functional materials: An integrated platform for applied technologies. *J. Electrochem. Soc.* **2018**, *165*, B3137–B3156, doi:10.1149/2.0191808jes.

3. Portier, J.; Choy, J.H.; Subramanian, M.A. Inoganic-organic-hybrids as precursors to functional materials, Int. *J. Inorg. Mater.* **2001**, *3*, 581–592, doi:10.1016/S1466-6049(01)00103-9.
4. Müller, K.; Bugnicourt, E.; Latorre, M.; Jorda, M.; Echegoyen Sanz, Y.; Lagaron, J.; Miesbauer, O.; Bianchin, A.; Hankin, S.; Bölz, U.; et al. Review on the processing and properties of polymer nanocomposites and nanocoatings and their applications in the packaging, automotive and solar energy fields. *Nanomaterials* **2017**, *7*, 74, doi:10.3390/nano7040074.
5. Egger, P.; Sorarù, G.D.; Diré, S. Sol-gel synthesis of polymer-YSZ hybrid materials for SOFC technology. *J. Eur. Ceram. Soc.* **2004**, *24*, 1371–1374, doi:10.1016/S0955-2219(03)00520-X.
6. MacEdo, D.A.; Cesário, M.R.; Cela, B.; Melo, D.M.A.; Paskocimas, C.A.; Martinelli, A.E.; Nascimento, R.M. Influence of polymerizing agent on structure and spectroscopic properties of nano-crystalline $La_{0.8}Sr_{0.2}MnO_3$ powders. *Cryst. Res. Technol.* **2010**, *45*, 1166–1170, doi:10.1002/crat.201000224.
7. Farhadian Azizi, K.; Bagheri-Mohagheghi, M.M. Transition from anatase to rutile phase in titanium dioxide (TiO_2) nanoparticles synthesized by complexing sol-gel process: Effect of kind of complexing agent and calcinating temperature. *J. Sol-Gel Sci. Technol.* **2013**, *65*, 329–335, doi:10.1007/s10971-012-2940-2.
8. Kozuka, H.; Takenaka, S.; Tokita, H.; Hirano, T.; Higashi, Y. ; Hamatani, T. Stress and cracks in gel-derived ceramic coatings. *J. Sol-Gel Sci. Technol.* **2003**, *26*, 681–686.
9. Park, W.-K. ; Kim, J.-Y.; Kim, S.-R.; Kim, T.; Iwasaki, M. Fabrication of a PVP (polyvinylpyrrolidone)-assisted TiO_2 film using a high-concentrated TiO2 nano sol and its optical properties. *J. Ceram. Soc. Jpn* **2011**, *119*, 745–751, doi:10.2109/jcersj2.119.745.
10. Tamrakar, R.K.; Bisen, D.P.; Robinson, C.S.; Sahu, I.P.; Brahme, N. Ytterbium doped gadolinium oxide (Gd_2O_3:Yb^{3+}) phosphor: Topology, morphology, and luminescence behaviour. *Indian J. Mater. Sci.* **2014**, *2014*, 396147, doi:10.1155/2014/396147.
11. Rath, M.K.; Acharya, S.K.; Kim, B.H.; Lee, K.T.; Ahn, B.G. Photoluminescence properties of sesquioxide doped ceria synthesized by modified sol-gel route. *Mater. Lett.* **2011**, *65*, 955–958, doi:10.1016/j.matlet.2011.01.004.
12. Zhang, H.; Chen, J.; Guo, H. Electrospinning synthesis and luminescent properties of Lu_2O_3:Eu^{3+} nanofibers. *J. Rare Earths* **2010**, *28*, 232–235, doi:10.1016/S1002-0721(10)60331-6.
13. Li, R.; Gai, S.; Wang, L.; Wang, J.; Yang, P. Facile synthesis and multicolor luminescent properties of uniform Lu_2O_3:Ln (Ln = Eu^{3+}, Tb^{3+}, Yb^{3+}/Er^{3+}, Yb^{3+}/Tm^{3+}, and Yb^{3+}/Ho^{3+}) nanospheres. *J. Colloid Interface Sci.* **2012**, *368*, 165–171, doi:10.1016/j.jcis.2011.10.026.
14. Zych, E.; Trojan-Piegza, J.; Kępiński, L. Homogeneously precipitated Lu_2O_3:Eu nanocrystalline phosphor for X-ray detection. *Sens. Actuators B Chem.* **2005**, *109*, 112–118, doi:10.1016/j.snb.2005.03.006.
15. Zych, E.; Trojan-Piegza, J.; Dorenbos, P. Radioluminescence of Lu_2O_3:Eu nanocrystalline powder and vacuum-sintered ceramic. *Radiat. Meas.* **2004**, *38*, 471–474, doi:10.1016/j.radmeas.2004.03.027.
16. Jia, G.A.; You, H.P.; Zheng, Y.H.; Liu, K.; Guo, N.; Zhang, H.J. Synthesis and characterization of highly uniform Lu_2O_3:Ln^{3+} (Ln = Eu, Er, Yb) luminescent hollow microspheres. *CrystEngComm* **2010**, *12*, 2943–2948, doi:10.1039/b924916h.
17. Jung, K.Y.; Lee, H.W.; Jung, H.K. Luminescent properties of (Sr, Zn)Al_2O_4:Eu^{2+}, Bi^{3+} particles as a potential green phosphor for UV LEDs. *Chem. Mater.* **2006**, *18*, 2249–2255, doi:Doi 10.1021/Cm060003w.
18. Wu, X.; Liang, Y.; Chen, R.; Liu, M.; Li, Y. Preparation and photoluminescence properties of Y_2O_3: Eu, Bi phosphors by molten salt synthesis for white light-emitting diodes. *J. Mater. Sci.* **2011**, *46*, 5581–5586, doi:10.1007/s10853-011-5508-6.
19. Kang, F.; Hu, Y.; Wu, H.; Ju, G.; Mu, Z.; Li, N. Luminescence investigation of Eu^{3+}–Bi^{3+} co-doped $CaMoO_4$ phosphor. *J. Rare Earths* **2011**, *29*, 837–842, doi:10.1016/S1002-0721(10)60552-2.
20. Takeshita, S.; Isobe, T.; Sawayama, T.; Niikura, S. Low-temperature wet chemical precipitation of YVO_4:Bi^{3+},Eu^{3+} nanophosphors via citrate precursors. *Prog. Cryst. Growth Charact. Mater.* **2011**, *57*, 127–136, doi:10.1016/j.pcrysgrow.2011.10.007.
21. Li, S.; Li, X.; Deng, K.; Wei, X.; Chen, Y.; Yin, M. Luminescent properties of $LuVO_4$: Bi^{3+}, Eu^{3+} red phosphor for light-emitting diodes. *J. Nanosci. Nanotechnol.* **2014**, *14*, 3631–3634, doi:10.1166/jnn.2014.8008.
22. Neeraj, S.; Kijima, N.; Cheetham, A.K. Novel red phosphors for solid state lighting; The system $Bi_xLn_{1-x}VO_4$; Eu^{3+}/Sm^{3+}(Ln = Y, Gd). *Solid State Commun.* **2004**, *131*, 65–69, doi:10.1016/j.ssc.2004.03.050.
23. Chen, X.; Zheng, Z.; Teng, L.; Wei, R.; Hu, F.; Guo, H. Self-calibrated optical thermometer based on luminescence from $SrLu_2O_4$:Bi^{3+},Eu^{3+} phosphors. *RSC Adv.* **2018**, *8*, 35422–35428, doi:10.1039/C8RA06358C.

24. Wang, W.; Sun, Z.; He, X.; Wei, Y.; Zou, Z.; Zhang, J.; Wang, Z.; Zhang, Z.; Wang, Y. How to design ultraviolet emitting persistent materials for potential multifunctional applications: A living example of a $NaLuGeO_4:Bi^{3+}$, Eu^{3+} phosphor. *J. Mater. Chem. C* **2017**, *5*, 4310–4318, doi:10.1039/c6tc05598b.
25. Kennedy, I.M.; Koivunen, M.M.; Gee, S.M.; Cummins, C.M.; Perron, R.M.; Dosev, D.M.; Hammock, B.D. Nanoscale fluoro-immuno assays with lanthanide oxide nanoparticles. *Proc. SPIE* **2004**, *5593*, 329–339, doi:10.1117/12.571483.
26. Ahmed, A.; Rushworth, J.V.; Hirst, N.A.; Millner, P.A. Biosensors for whole-cell bacterial detection. *Clin. Microbiol. Rev.* **2014**, *27*, 631–646, doi:10.1128/CMR.00120-13.
27. Lenczewska, K.; Stefanski, M.; Hreniak, D. Synthesis, structure and NIR luminescence properties of Yb^{3+} and Bi^{3+}-activated vanadate $GdVO_4$. *J. Rare Earths* **2016**, *34*, 837–842, doi:10.1016/S1002-0721(16)60103-5.
28. Shang, Y.; Hao, S.; Yang, C.; Chen, G. Enhancing solar cell efficiency using photon upconversion materials. *Nanomaterials* **2015**, *5*, 1782–1809, doi:10.3390/nano5041782.
29. Mackenzie, J.D.; Bescher, E.P. Physical properties of sol-gel coatings. *J. Sol-Gel Sci. Technol.* **2000**, *19*, 23–29, doi:10.1023/A:1008701903087.
30. Jeon, H.J.; Yi, S.C.; Oh, S.G. Preparation and antibacterial effects of Ag–SiO_2 thin films by sol-gel method. *Biomaterials* **2003**, *24*, 4921–4928, doi:10.1016/S0142-9612(03)00415-0.
31. Guo, H.; Yin, M.; Dong, N.; Xu, M.; Lou, L.; Zhang, W. Effect of heat-treatment temperature on the luminescent properties of Lu2O3:Eu film prepared by Pechini sol-gel method. *Appl. Surf. Sci.* **2005**, *243*, 245–250, doi:10.1016/j.apsusc.2004.09.069.
32. Xie, J.; Deng, L.; Shi, Y.; Xie, J.; Qiu, H.; Song, G. The influence of Pr^{3+} co-doping on the luminescent properties of Lu_2O_3:5 mol % Eu films. *J. Lumin.* **2011**, *131*, 970–974, doi:10.1016/j.jlumin.2011.01.004.
33. Yamamoto, Y.; Kamiya, K.; Sakka, S. Study on the properties of coating films prepared from metal alkoxides. *J. Ceram. Soc. Jpn.***1982**, *90*, 328–333.
34. Kozuka, H. Stress evolution on gel-to-ceramic thin film conversion. *J. Sol-Gel Sci. Technol*. **2006**, *40*, 287–297, doi:10.1007/s10971-006-9213-x.
35. Liu, X.; Han, K.; Gu, M.; Huang, S.; Liu, B.; Ni, C. Optical properties of $GdTaO_4:Eu^{3+}$ thick films prepared from a PVP-containing solution. *Appl. Surf. Sci.* **2009**, *255*, 4680–4683, doi:10.1016/j.apsusc.2008.12.026.
36. Rho, Y.H.; Dokko, K.; Kanamura, K. Li^+ ion diffusion in $LiMn_2O_4$ thin film prepared by PVP sol-gel method. *J. Power Sources* **2006**, *157*, 471–476, doi:10.1016/j.jpowsour.2005.07.050.
37. Morales Ramírez, A.; García Hernández, M.; Yepez Ávila, J.; García Murillo, A.; Carrillo Romo, F.; De La Rosa, E.; Garibay Febles, V.; Reyes Miranda, J. Eu^{3+}, Bi^{3+} codoped Lu_2O_3 nanopowders: Synthesis and luminescent properties. *J. Mater. Res.* **2013**, *28*, 1365–1371, doi:10.1557/jmr.2013.91.
38. Chi, Y.; Chuang, S.S.C. Infrared and TPD Studies of nitrate adsorbed on Tb_4O_7, La_2O_3, BaO, and MgO/γ-Al_2O_3. *J. Phys. Chem. B.* **2000**, *104*, 4773–4683, doi:10.1016/j.ijhydene.2015.05.098.
39. Tu, W.; Zuo, X.; Liu, H. Study on the Interaction between polyvinylpyrrolidone and platinum metals during the formation of the colloidal metal nanoparticles. *Chin. J. Polym. Sci.* **2008**, *26*, 23–29, doi:10.1142/S0256767908002625.
40. Mcdevitt, N.T.; Baun, W.L. Infrared absorption study of metal oxides in the low frequency region (700–240 cm^{-1}). *Spectrochim. Acta* **1964**, *20*, 799–808, doi:10.1016/0371-1951(64)80079-5.
41. Koczkur, K.M.; Mourdikoudis, S.; Polavarapu, L.; Skrabalak, S.E. Polyvinylpyrrolidone (PVP) in nanoparticle synthesis. *Dalt. Trans.* **2015**, *44*, 17883–17905, doi:10.1039/c5dt02964c.
42. Kandhasamy, S.; Pandey, A.; Minakshi, M. Polyvinylpyrrolidone assisted sol-gel route $LiCo_{1/3}Mn_{1/3}Ni_{1/3}PO_4$ composite cathode for aqueous rechargeable battery. *Electrochim. Acta* **2012**, *60*, 170–176, doi:10.1016/j.electacta.2011.11.028.
43. Fukada, H.; Konagai, M.; Ueda, K.; Miyata, T.; Minami, T. Photoluminescent and electroluminescent characteristics of various Bi-activated niobate-based oxide phosphor thin films. *Thin Solid Films* **2009**, *517*, 6054–6057, doi:10.1016/j.tsf.2009.04.064.
44. Liu, H.Q.; Wang, L.L.; Chen, S.Q.; Zou, B. Effect of concentration on the luminescence of Eu^{3+} ions in nanocrystalline La_2O_3. *J. Lumin.* **2007**, *126*, 459–463, doi:10.1016/j.jlumin.2006.09.001.
45. Medina, D.Y.; Orozco, S.; Hernandez, I.; Hernandez, R.T.; Falcony, C. Characterization of europium doped lanthanum oxide films prepared by spray pyrolysis. *J. Non-Cryst. Solids* **2011**, *357*, 3740–3743, doi:10.1016/j.jnoncrysol.2011.07.021.

46. Su, J.; Zhang, Q.L.; Shao, S.F.; Liu, W.P.; Wan, S.M.; Yin, S.T. Phase transition, structure and luminescence of Eu:YAG nanophosphors by co-precipitation method. *J. Alloy. Compd.* **2009**, *470*, 306–310, doi:10.1016/j.jallcom.2008.02.045.
47. Binnemans, K. Interpretation of europium (III) spectra. *Coord. Chem. Rev.* **2015**, *295*, 1–45, doi:10.1016/j.ccr.2015.02.015.
48. Wang, L.-L.; Wang, Q.-L.; Xu, X.-Y.; Li, J.-Z.; Gao, L.-B.; Kang, W.-K.; Shi, J.-S.; Wang, J. Energy transfer from Bi^{3+} to Eu^{3+} triggers exceptional long-wavelength excitation band in $ZnWO_4$:Bi^{3+}, Eu^{3+} phosphors. *J. Mater. Chem. C* **2013**, *1*, 8033–8040, doi:10.1039/c3tc31160k.
49. Li, K.; Lian, H.; Shang, M.; Lin, J. A novel greenish yellow-orange red $Ba_3Y_4O_9$:Bi^{3+}, Eu^{3+} phosphor with efficient energy transfer for UV-LEDs. *Dalt. Trans.* **2014**, *44*, 20542–20550, doi:10.1039/x0xx00000x.
50. Abedrabbo, S.; Lahlouh, B.; Fiory, A.T. Analytical study of thermal annealing behaviour of erbium emission in Er_2O_3-sol–gel silica films. *J. Phys. D Appl. Phys.* **2011**, *44*, 315401, doi:10.1088/0022-3727/44/31/315401.
51. Sahu, B.S.; Delachat, F.; Slaoui, A.; Carrada, M.; Ferblantier, G.; D. Muller, Effect of annealing treatments on photoluminescence and charge storage mechanism in silicon-rich SiN_x:H films. *Nanoscale Res. Lett.* **2011**, *6*, 178, doi:10.1186/1556-276X-6-178.
52. Smith, T.; Guild, J. The C.I.E. colorimetric standards and their use. *Trans. Opt. Soc.* **1931**, *33*, 73, doi:10.1088/1475-4878/33/3/301.
53. Lou, Z.; Hao, J. Cathodoluminescence of rare-earth-doped zinc aluminate films. *Thin Solid Films* **2004**, *450*, 334–340, doi:10.1016/j.tsf.2003.11.294.
54. Carnall, W.T.; Fields, P.R.; Rajnak, K. Electronic energy levels of the trivalent lanthanide aquo ions. III. Tb^{3+}. *J. Chem. Phys.* **1968**, *49*, 4447–4449, doi:10.1063/1.1669895.
55. Chang, Y.S.; Lin, H.J.; Chai, Y.L.; Li, Y.C. Preparation and luminescent properties of europium-activated $YInGe_2O_7$ phosphors. *J. Alloy. Compd.* **2008**, *460*, 421–425, doi:10.1016/j.jallcom.2007.05.060.
56. Inokuti, M.; Hirayama, F. Influence of energy transfer by the exchange mechanism on donor luminescence. *J. Chem. Phys.* **1965**, *43*, 1978–1989, doi:10.1063/1.1697063.